Improvements of Organic Photodetectors for VLC Using a New Active Layer, Focal Lens, and a Transimpedance Amplifier

Pablo Corral[1, *], Fernando Rodriguez-Mas[1], Guillermo De Scals[2], David Valiente[1], Juan Carlos Ferrer[1], Susana Fernandez de Avila[1]
[1]Department of Communications Engineering, Universidad Miguel Hernandez de Elche, Avda. Universidad S/N, 03202 Elche, Spain
[2]Department of Applied Physics, Universidad Miguel Hernandez de Elche, Avda. Universidad S/N, 03202 Elche, Spain
pcorral@umh.es

***Abstract*—Beyond 5G networks, and for short distance but high-speed communication systems, there is an incipient growing interest in visible light communications (VLC). Furthermore, it is an interesting alternative within the framework of the Internet of Things (IoT). However, there is a problem on the part of the receiver in these systems, motivated by the non-existence of photovoltaic elements used particularly for this purpose. Because of their simplicity and small investment, organic-type photodetectors have a high capacity for use in VLC systems. With a structure of polymers represented by an organic photodetector fabricated with poly (3-hexylthiophene) (P3HT) and a bulk heterojunction active layer of phenyl-C61-butyric acid methyl ester (PCBM) and commercial LEDs, we show our system in this paper. The main novelty of this work is in reception. With different upgrade using a new active layer or adding a focal lens or inserting a transimpedance amplifier, we have achieved improved performance results related to voltage and distance, with an increase of more than 40 %, and Bit Error Rate (BER) by modifying the active layer concentration with respect to results obtained in a former work. Also, we have tested the use of a transimpedance amplifier to obtain the best results in distances of 12 cm to 20 cm and a focal lens with the same objective of improving the BER in critical environments, where the Signal-to-Noise Ratio (SNR) is close to zero. To conclude, these modifications show that it is possible to increase the main parameters of our system to be useful in VLC systems.**

***Index Terms*—Visible light communication; Organic materials; Wireless communication; Solar panels.**

I. INTRODUCTION

A relevant technology that serves as a complement to current radio frequency (RF) systems, within wireless optical communications, is particularizing visible light communications (VLCs), since they have the possibility of being an element of change in some environments, such as interiors, where its extremely large bandwidth exhibits great advantages for the final performance. In the final performance, it is appreciated that the bandwidth presents high advantages. On the other hand, it can be installed from vehicle to vehicle being in a free environment (V2V) and from vehicle to rest (V2X), as well as in other uses of high speed of short-range data, apart from fifth-rate networks generation (B5G). Using the modulation capacity of the light using the LED light diodes, we can say that the VLC technique is supported, to transmit the data. This transmission does not affect to human eyes and, in some cases, neither to ambient light. Obviously, this presents us with an option for secure, high-speed [1] and secure communications using existing lighting infrastructure.

VLC comprises optical wireless systems standardized by IEEE 802.15.7 [1]. It defines a physical layer (PHY) and a medium access control (MAC) sublayer for optical wireless personal area networks (OWPAN) that employ light wavelengths from 190 nm to 10 μm [2]. The standardized physical layer supports six different physical types (PHY), three of them, PHY IV, V, and VI, are robust against impairments caused by interference and noise from different sources, such as ambient light.

Currently, the Internet of Things (IoT) promotes effective economic growth with improved quality of life through interconnected devices [3]–[6]. In this context, it is important to use a system that can handle with a large number of devices that operate simultaneously. With our focus on receptor elements, we know that the incipient request for high flexibility, clarity, and cost-effective manufacturing systems is fostering the development of organic but P3HT: PCBM-based photodetector systems, versus common silicon-based ones.

Different types of high-performance photon photodetectors should be considered as examples of developments in this area of work. For instance, those based on germanium photodetector arrays integrated using transimpedance amplifiers [7], or plasmon-enhanced quantum light-emitting and optical devices [8], or a new class of photodetectors with high gain, which improves the responsivity and the noise equivalent power [9].

In our case, the use of organic materials in our devices allows for a creation of a low-cost VLC system with wide availability and easy commercial deployment due to the

Manuscript received 19 February, 2022; accepted 30 May, 2022.

integration of a self-powered organic photodetector [10]–[12]. Finally, this system is not affected by ambient light or other interference. The range of power consumption, as well as the low cost, make them attractive attributes for mass manufacturers and IoT devices.

The structure of this paper is as follows. Section II describes motivation, gives sufficient background on our work, and emphasizes state-of-the-art. Section III focuses on the material and methods used in this work. Section IV describes the main results obtained, comparing the previous device called "OPD_1" with the new devices that modify the active layer or add a new transimpedance amplifier called "OPD_2" and "OPD_3", respectively. In Section V, we show the discussion, and finally, the conclusions are included in Section VI.

II. Related Works

In recent years, some authors have shown results to enhance the transmission performance of organic photodetectors using pre-distortion scheme [13] or the optimisation of low-cost visible light communications through OLEDs in transmission [14]. In another example of a manuscript related to our work, we can find a comparative study of organic photodetectors based on PH3T and PTB7 for visible light communications [15]. Or, e.g., a new photodetector structure combining a thinned CdTe film with a lead-free Perovskite photoelectric film [16]. In our paper, we have shown an improvement of visible light communication using an ultra low-cost LED in transmission and different upgrade in reception using a new active layer or adding a focal lens or inserting a transimpedance amplifier.

III. Materials and Methods

A. Description of the System

With the idea of achieving improvements in communications, three experiments were carried out: in the first, the concentration of the active layer was modified, in the second configuration, a focal lens was added with the intention of collimating the beam, and in the third configuration, a transimpedance amplifier was added to increase the received voltage.

In Fig. 1, the experimental system scheme is exposed to be able to detect the VLC without improving both the maximum allowed frequency and the maximum allowed distance.

As we can see in Fig. 1, the self-powered organic photo detector (OPD) is composed of cells with different sizes, with diameters from 3,5 mm to 4,5 mm. We have used a unique high luminosity LED chip as the transmitter; it is a white-light phosphor-based LED with a correlated colour temperature (CCT) of 5500 K. On the one hand, to generate the signals, we have used an arbitrary waveform generator (AWG, Digilent ® Analog Discovery 2) applied to the LED. This device has an analog bandwidth of 12 MHz and a sample rate of 100 MSample/s. To detect signals, the OPD was linked to a real-time oscilloscope (RTO, Digilent ® Analog Discovery 2). The most relevant parameters of the RTO are the 100 MSample/s sampling frequency and an analog bandwidth of 30 MHz.

Fig. 1. The first experimental configuration can be seen in the block diagram. For this, an RTO, a LED, an OPD, and an AWG were used. All the abbreviations are explained in the text above.

To find out the further distance that the VLC system supports, it was decided to add a focal lens for that purpose, as we can see in the experimental configuration of the OPD. A single LED chip, similar to the first configuration, was used as a transmitter in the experiment.

We have generated the Manchester code signals with an ATmega 328 microcontroller which act as an input to the LED with a frequency of 1 KHz. A special case of encoding is Manchester encoding, which is done by binary phase shift (BPSK), where at each bit time there is a transition between two signal levels.

As we can see in Fig. 2, we have added a lens with 30 mm of focal length and a diameter of 2.54 cm. To detect and acquire the transmitted signal, we self-powered an OPD joined to the ATmega 328 microcontroller. In this experiment, the results were recorded and monitored on the computer. The ATmega 328 microcontroller model had a sampling and clock rate of 16 MHz and 10 KSample/s.

Fig. 2. The experimental second setup can be seen through a block diagram, using an ATmega 328 microcontroller in transmission and reception, a LED, a focal lens, the OPD, and a computer.

Finally, in Fig. 3, we can see the block diagram once it is included, with the purpose of obtaining the maximum allowed voltage of the system, a transimpedance amplifier (TIA) based on an operational amplifier chip (LT1028). In the present experiment, based on the same LED transmitter that was used in the first and the second setups, an AWG was used applied to this LED. This device has an analog bandwidth of 12 MHz and a sample rate of 100 MSample/s. For the purpose of detecting the signals, the self-powered OPD was connected to an RTO. The most relevant parameters of the RTO related to analog bandwidth and sampling frequency are the same as in the first configuration.

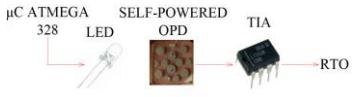

Fig. 3. For the third configuration of the experiment, the present block diagram was used, including an AWG, a LED, an OPD, a TIA, and an RTO. TIA: transimpedance amplifier.

The use of a transimpendance amplifier ensures sufficient performance to meet all major requirements of the system, such as improvements in distance, frequency, or BER [17].

B. Materials

Regarding the manufacturing of the organic photodetectors, we have used chlorobenzene, [6,6]-phenyl-

C61-butyric (PCBM), poly(3-hexylthiophene) (P3HT), and poly(3,4-ethylenedioxythiophene):poly(styrene sulfonate) (PEDOT:PSS, 1.3 % water solution). To clean the substrates, we used 1-2-4 trichlorobenzene, acetone, and isopropyl alcohol. All materials were acquired from Sigma-Aldrich (Darmstadt, Germany). And all materials were used without further purification.

C. Methods

By means of the technique of coating by rotation, OPDs were carried out, since this manufacturing technique facilitates the generation of the structure by depositing the material in thin layers. The organic formation of the elements resulted as follows: TO/PEDOT: PSS/P3HT: PCBM/Al. Using ultrasonic-type chemical baths, commercial glass substrates that had a slim layer of indium tin oxide (ITO) were cleaned. They were then introduced, respectively, in 1-2-4-trichlorobenzene, acetone, and isopropyl alcohol for 20 minutes and dried using N_2. With a speed of 6,000 rpm, the PSS was coated by centrifugation on the glass-ITO substrate, PEDOT. PEDOT was used for all organic-type receptors and PSS as the hole carrier layer. Then PEDOT:PSS was dried for 60 minutes at 120 °C. Using an active layer PCBM (mass ratio 1:1), a mixture of P3HT was used and dissolved in chlorobenzene at 10 mg/ml and the active layers were spin-coated at 500 revolutions per minute and were evaporated at 80 °C for sixty minutes.

After that, the last process of metallization was carried out using aluminium. The description of the metallization system turned out as follows. Using a high vacuum chamber, the aluminum was evaporated, until 200 nm was achieved. In a sequential way, a travel ramp was started as a process. Up to 120 °C, the devices were taken. After this, they were held for 120 seconds. The devices were finally cooled to room temperature.

To achieve optical characterization, a Triax 190 was used as a monochromator and as a thermoelectrically cooled multi-channel Symphonic Charge-Coupled Device (CCD) detector from Horiba Jobin Yvon.

As an emitting device, a high-luminosity White LED (HL-White) was selected. This type of LED was used in our previous research, where its better behaviour compared to other commercial LEDs was verified [18].

Figure 4 shows the intensity spectrum of the HL-White LED. In this picture, we can observe that the spectrum is composed of two contributions. The first was located at a low wavelength. It is a narrow peak with its maximum emission at 465 nm. The other contribution, at a higher wavelength, was a broad peak in relation to the first one, and its maximum emission peak was located at 562 nm. These differences can be observed in Table I. In this table, the full width at half maximum (FWHM) is also detailed. To characterize the LED appropriately, the irradiance was measured.

According to the characterization of the photodetector, the curves of current density versus voltage (J-V) of the OPDs were taken working with a Keithley 2400 Sourcemeter equipment. The measurement conditions were light conditions (100 mW/cm^2, 25 °C) represented by a xenon arc lamp and an AM1.5G filter under dark conditions.

The results can be observed in Table II.

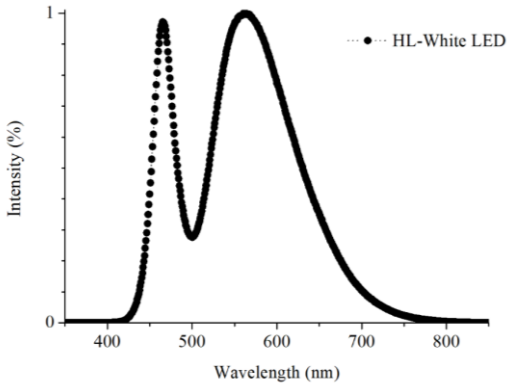

Fig. 4. Relative intensity spectrum of high-luminosity White LED (HL-White).

TABLE I. OPTICAL CHARACTERISTICS OF HIGH-LUMINOSITY LED (HL-WHITE). EMISSION PEAK IN NM, FULL WIDTH AT HALF MAXIMUM (FWHM).

LED	Emission Peak (nm)	FWHM (nm)
HL-White	465	27
	562	120

TABLE II. ELECTRICAL PARAMETERS OF THE REFERENCE OPD.

OPD	J_{SC} (mA/cm^2)	V_{OC} (V)	P_{MPP} (mW)	FF (%)	η (%)
OPD_2	4.1	0.52	0.080	30.5	0.64

Based on the studies carried out in our previous work [16], the OPD bandwidth could be calculated as indicated in (1)

$$BW = \frac{0.35}{t_{rise}}. \quad (1)$$

As the rise time depends on the wavelength of the LED, the measurements were performed with HL-White LED, Table III. This rise time is the time that a signal considers to vary from a determined low value to a determined high value, expressed in percentages, normally between 10 % and 90 % [19]. Again, the real-time oscilloscope (RTO, Digilent ® Analog Discovery 2) was used for signal detection.

TABLE III. ELECTRICAL PARAMETERS OF THE REFERENCE OPD.

OPD	Rise Time (ms)	Bandwidth (kHz)
OPD_2	0.094	3.71

For an ideal low-pass filter, the rise time is 0.44/BW but, under normal conditions, the rise time and 3 dB bandwidth are inversely proportional, with a proportionality constant of ~0.35 when the system's response resembles that of an RC low-pass filter with a simple pole [20]. The bandwidth of HL-White LED was used as a bandwidth reference, as it is higher than the OPD bandwidth [21]. The capacitance of our OPD can be calculated from the value of the rise time, assuming that the value of the resistance is well known.

IV. RESULTS

This section analyses the performance of our VLC system

when the OPDs presented in Section III-A are integrated. In the first system, a periodic sinusoidal signal was used to power the HL-White LED, whereas the frequency of the periodic signal was modified. As a result, the maximum supported frequency of the system was determined, Fig. 5. The acquisition of the measurements was carried out with a load resistance of 1 MΩ. The system block diagram was initially presented in Fig. 1. With a voltage at the potential input of 3.3 V, the AWG is fed into the transmission process.

The result of 1.5 mV was the lowest level detected by the RTO during reception. These data have been compared with the results obtained in our previous investigation [18]. In this previous research, the communication system is the same as that used in the current study. From now on, the data from the OPD we used in the previous study is named "OPD_1".

The comparison between the previous OPD (OPD_1) and the current OPD (OPD_2) shows an increase in OPD_2 voltage with respect to OPD_1 of 269 % at 1 kHz. And these characteristics appear not only at 1 kHz, but also at 2 kHz and 5 kHz, where the results get better than in OPD_1 in short distances, as noticed in Table IV. Furthermore, the emitter-detector distance at 1 kHz where the system works correctly increases by 7 cm thanks to the use of OPD_2. So, the OPD_2 reaches up to 20 cm from transmitter to receiver with an enough level of voltage in the communication system. The improvements in the efficiency of the organic photodetectors allowed us to reach these positive results.

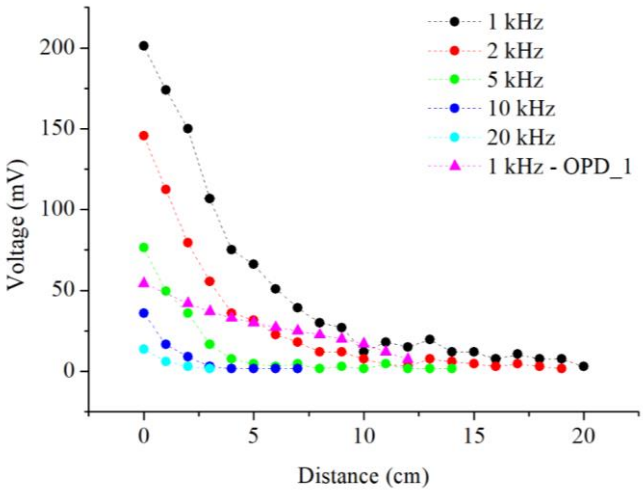

Fig. 5. Maximum supported distance of the system employing OPD_2 at different frequencies and OPD_1 at 1 kHz.

TABLE IV. INCREASE OF VOLTAGE AT 0 CM BETWEEN OPD_2 AND OPD_1 AT 1 KHZ, 2 KHZ, AND 5 KHZ.

Frequency	OPD_2 (mV)	Increase (%)
1 kHz	201.18	269.81
2 kHz	145.55	167.55
5 kHz	76.5	40.63

The power ratio that affects the device and the maximum generated defines the efficiency represented in Table II. In the two studies carried out, the results for the OPD, OPD_2, and OPD_1 of the incident type power were the same, respectively. Therefore, the increase in efficiency was translated into an increase in the maximum power generated by the photodetector. Then, under the same conditions, OPD_2 produces more power than OPD_1. These two discussed improvements are derived from the increase in efficiency, from 0.01 % [18] to 0.64 % (Table II).

The OPD_2 and OPD_1 structure was the same and the manufacturing conditions (revolution, drying temperature, and time of the spin-coating process) were also the same. There exists only one difference in the fabrication process of the photodetectors: the active layer concentration was modified for OPD_2. The concentration changed from 10 mg/ml [18] to 20 mg/ml. Increasing the concentration of the active layer increases the absorption [22], [23]. The quantity of photons collected by the active layer of OPD was directly proportional to the absorption of the layer. Because of the increase in the number of collected photons, the current density is higher because more electrons were generated. Therefore, efficiency and absorption were directly related [22].

Using the RTO, a histogram is obtained, which helps us to calculate the quality factor (Q) of the received signal. The result obtained shows us the affirmation of an improvement in the optical channel with respect to its performance, VLC at 1 kHz, in contrast to [18]. Using (2),

$$Q = \frac{I_1 - I_0}{\sigma_1 + \sigma_0}, \tag{2}$$

where $\sigma_{0,1}$ and $I_{0,1}$ indicate, respectively, half width at half maximum (HWHM) and maximum peak of the Gaussian distribution of the current based on the value of optical power on the photodetector for level 0 and 1 [24], [25]. Moreover, (3) permits one to calculate the optical bit error rate (BER) of the VLC [26]

$$BER(Q) = \frac{1}{2} erfc\left(\frac{Q}{\sqrt{2}}\right). \tag{3}$$

In [18], the best BER was 10^{-7} with a Signal-to-Noise

Ratio (SNR) of 35.58 dB, whereas the current OPD_2 demonstrates a best BER of 8.79 × 10^{-18} with a SNR of 29.43 dB, as denoted in Fig. 6. In most cases of real environments, thermal noise is the most important contribution of noise in the receiver and the SNR becomes, as we can see in (4)

$$SNR = \frac{R_L R^2 P_{in}^2}{4k_B T F_n \Delta f}. \quad (4)$$

So, the SNR changes with P_{in}^2 in the thermal-noise limit, and normally we use a high-impedance or transimpedance front end because of the dependence with the load resistance. The thermal noise result is normally measured using the noise equivalent power (NEP) which is stated as the minimum optical power per unit bandwidth necessary to obtain SNR = 1. It is also defined as the optical power needed to generate a detector current equal to the Root Mean Square (RMS) noise current in unit bandwidth (BW= 1 Hz) [27]. Characteristic values of NEP are within the range of 1 pW/Hz ½–10 pW/Hz ½. NEP is given by (5)

$$NEP = \frac{P_{in}}{\sqrt{\Delta f}} = \left(\frac{4k_B T F_n}{R_L R^2} \right)^{1/2} = \frac{h\nu}{\eta q} \left(\frac{4k_B T F_n}{R_L} \right). \quad (5)$$

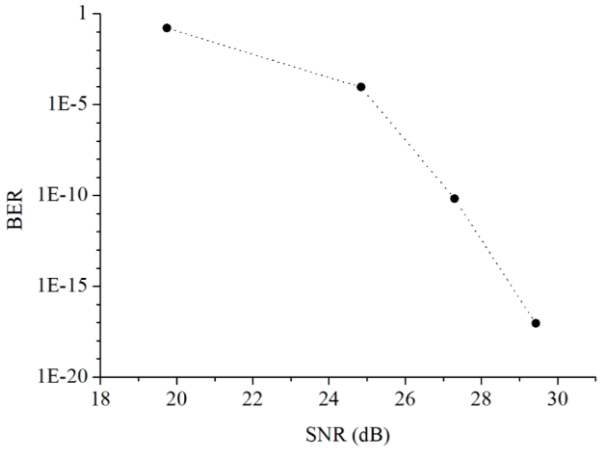

Fig. 6. BER versus SNR for OPD_2 with the high-luminosity White LED.

As we can see in Fig. 6, as the SNR increases, the BER improves. This decrease in BER is more accentuated than in previous results [18] and confirms the improvement obtained with increasing concentration.

In the second experimental setup, we have added a lens of 30 mm of focal length and a diameter of 2.54 cm between the LED and the photodetector. To determine the focal length of a concave lens, we need to collimate our beam to be focused on a single spot.

As we can see in Fig. 7, using a focal lens with a fixed distance of 30 mm to the LED proves better results than the previous experimental setup. This improvement is significantly important in lower SNR, where the first experimental setup does not work very efficiently. It could be very interesting to apply this to critical environments where the SNR is close to zero.

This solution is optimal at a distance between the lens and the LED of 3 cm; as we move away from that distance, the beam tends to diverge and the result is not so efficient, although it is still better than without using the lens.

Finally, in Table V, we can see the results obtained for the third experimental setup, where a transimpedance amplifier (TIA) based on the operational amplifier chip LT1028 is added. TIA is useful to increase the current output of the devices to a usable voltage [28]. This chip block separates the voltage of the operational amplifier in the output and thus provides a small value of the impedance to the photodiode. In that case, using the TIA, we increased the maximum voltage to 137.76 %.

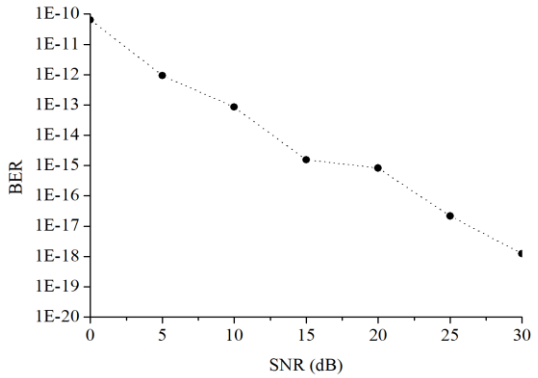

Fig. 7. BER versus SNR for OPD_2 with high-luminosity White LED using a fixed focal lens. On the right side, the LED below, the lens in the middle, and the OPD above can be observed.

TABLE V. INCREASE OF VOLTAGE AT 1 KHZ BETWEEN OPD_2 AND OPD_3 AT 0 CM, 1 CM, AND 2 CM.

Distance	OPD_2 (mV)	OPD_3 (mV)	Increase (%)
0 cm	201.18	478.33	137.76
1 cm	174.06	309.87	78.02
2 cm	149.95	242.34	61.61

In the last experiment, large improvements were achieved at small distances, but as the distance increased, the increase of the voltage decreased and the noise effect increased.

V. DISCUSSION

According to the results obtained from the previous experiments, the three different experimental setups have obtained better results and have demonstrated the value of these proposals. For example, in the first experimental setup, changing the concentration of the active layer in the OPD_2 from 10 mg/ml to 20 mg/ml allows up to 20 cm from transmitter to receiver with an enough level of voltage in the communication system. The improvements in the efficiency of the organic photodetectors made it possible to obtain these positive results.

In the second experimental setup, we have added a lens of 30 mm of focal length and a diameter of 2.54 cm between the LED and the photodetector achieving interesting results when the SNR is close to zero. Unfortunately, the limitation of this experimental setup is due to the distance; in that situation, the beam tends to diverge, and the result is not as efficient.

Finally, the third experiment setup includes a transimpedance amplifier that increases the voltage in

reception but is affected by distance and noise effect.

VI. CONCLUSIONS

The operational capacity of a low-cost VLC type system is demonstrated in this document based on a self-powered OPD manufactured with a structure based on P3HT: PCBM. The system is not affected by ambient light or other interference. In our paper, we have shown an improvement of a VLC using an ultra low-cost LED in transmission and a different upgrade in reception using a new active layer or adding a focal lens or inserting a transimpedance amplifier. In the basic structure of the OPD, we had improved its classical limitations by introducing changes in the active layer concentration to obtain an increase of 269.81 % in maximum voltage relative to the previous research. Another advantage is validated in terms of the maximum supported distance to detect the threshold signal. With the first structure, we get an increase of 8 cm, from 12 cm to 20 cm. After a focal lens is added, the results are better not only in distance but also in voltage and BER. Finally, including a transimpedance amplifier (TIA) based on the operational amplifier chip LT1028, we increased the maximum voltage by up to 137.76 % with respect to OPD_2. After the study, it has been concluded that the organic-type photodetectors, given their properties, could achieve improvements if new materials with high mobility of charge were developed, and making improvements in manufacturing. It is therefore that the response speed can be increased in organic-type devices.

As a future work, we are developing new active layers that allow us to work at higher frequencies for the transmission of images and videos in real time [29].

CONFLICTS OF INTEREST

The authors declare that they have no conflicts of interest.

REFERENCES

[1] "IEEE 802.15.7-2018 - IEEE Standard for Local and metropolitan area networks--Part 15.7: Short-Range Optical Wireless Communications", in *IEEE Std 802.15.7-2018 (Revision of IEEE Std 802.15.7-2011)*, pp. 1–407, 23 April 2019.

[2] E. Torres-Zapata, V. Guerra, J. Rabadan, M. Luna-Rivera, and R. Perez-Jimenez, "MAC/PHY comprehensive visible light communication networks simulation", *Sensors*, vol. 20, no. 21, p. 6014, 2020. DOI: 10.3390/s20216014.

[3] M. M. El Gamal, H. A. Fayed, M. H. Aly, N. E. Ismail, and A. Mokhtar, "Interactive internet of things based on dark light system for smart room", *Opt. Quant. Electron.*, vol. 52, art. no. 493, 2020. DOI: 10.1007/s11082-020-02614-z.

[4] W. Pawlikowski, A. Barmaki, M. Narimani, and S. Hranilovic, "Light-emitting commutating diodes for optical wireless communications within LED drivers", *IEEE Photon. J.*, vol. 12, no. 5, pp. 1–11, art. 7905111, 2020. DOI: 10.1109/JPHOT.2020.3020749.

[5] X. Bao, J. Dai, and X. Zhu, "Visible light communications heterogeneous network (VLC-HetNet): New model and protocols for mobile scenario", *Wireless Networks*, vol. 23, no. 1, pp. 299–309, 2017. DOI: 10.1007/s11276-016-1233-z.

[6] F. J. Estevez, J. M. Garcia, J. M. Castillo-Secilla, J. Gonzalez, and P. Gloesekoetter, "Enabling validation of IEEE 802.15.4 performance through a new dual-radio OMNeT++ model", *Elektronika ir Elektrotechnika*, vol. 22, no. 3, pp. 89–94, 2016. DOI: 10.5755/j01.eie.22.3.15321.

[7] C. Hoessbacher *et al.*, "Optical interconnect solution with plasmonic modulator and Ge photodetector array", *IEEE Photonics Technology Letters*, vol. 29, no. 21, pp. 1760–1763, 2017. DOI: 10.1109/LPT.2017.2723727.

[8] A. I. Fernandez-Domínguez, S. I. Bozhevolnyi, and N. A. Mortensen, "Plasmon-enhanced generation of nonclassical light", *ACS Photonics*, vol. 5, no. 9, pp. 3477–3451, 2018. DOI: 10.1021/acsphotonics.8b00852.

[9] L. Liu *et al.*, "Room-temperature high-gain long-wavelength photodetector via optical–electrical controlling of hot carriers in graphene", *Advanced Optical Materials*, vol. 6, no. 24, art. 1800836, 2018. DOI: 10.1002/adom.201800836.

[10] B. Arredondo *et al.*, "Visible light communication system using an organic bulk heterojunction photodetector", *Sensors*, vol. 13, no. 9, pp. 12266–12276, 2013. DOI: 10.3390/s130912266.

[11] C. Vega-Colado *et al.*, "An all-organic flexible visible light communication system", *Sensors*, vol. 18, no. 9, p. 3045, 2018. DOI: 10.3390/s18093045.

[12] E. López-Fraguas *et al.*, "Visible light communication system using an organic emitter and a perovskite photodetector", *Org. Electron.*, vol. 73, pp. 292–298, 2019. DOI: 10.1016/j.orgel.2019.06.028.

[13] C.-W. Chow, H.-Y. Wang, C.-H. Chen, H.-W. Zan, C.-H. Yeh, and H.-F. Meng, "Pre-distortion scheme to enhance the transmission performance of organic photo-detector (OPD) based visible light communication (VLC)", *IEEE Access*, vol. 6, pp. 7625–7630, 2018. DOI: 10.1109/ACCESS.2018.2805226.

[14] P. de Souza *et al.*, "High-bandwidth organic light emitting diodes for ultra-low cost visible light communication links", in *Proc. of 2018 20th International Conference on Transparent Optical Networks (ICTON)*, 2018, pp. 1–4. DOI: 10.1109/ICTON.2018.8473617.

[15] L. Salamandra *et al.*, "A comparative study of organic photodetectors based on P3HT and PTB7 polymers for visible light communication", *Organic Electronics*, vol. 81, art. 105666, 2020. DOI: 10.1016/j.orgel.2020.105666.

[16] I. M. Pandiev and M. P. Aleksandrova, "Dynamic FPAA-based mixed-signal processing circuit for thin-film CdTe/lead-free Perovskite photodetectors", *Elektronika ir Elektrotechnika*, vol. 27, no. 2, pp. 22–30, 2021. DOI: 10.5755/j02.eie.28751.

[17] A. Romanova and V. Barzdenas, "A review of modern CMOS transimpedance amplifiers for OTDR applications", *Electronics*, vol. 8, no. 10, p. 1073, Sep. 2019. DOI: 10.3390/electronics8101073.

[18] P. Corral, F. Rodríguez-Mas, J. L. Alonso, J. C. Ferrer, and S. Fernández de Ávila, "A low-cost IEEE 802.15.7 communication system based on organic photodetection for device-to-device connections", *Sensors*, vol. 20, no. 3, p. 714, 2020. DOI: 10.3390/s20030714.

[19] H. Ahmad, K. Thambiratnam, T. C. Leong, T. M. K. Thandavam, and R. Ramli, "Low-cost SWIR silicon-based graphene oxide photodetector", in *Proc. of 2019 IEEE 9th International Nanoelectronics Conferences (INEC)*, 2019, pp. 1–3. DOI: 10.1109/INEC.2019.8853864.

[20] J. Gowar, *Optical Communication System*, 2nd ed. New York: Prentice Hall, 1993.

[21] C.-L. Liao, C.-L. Ho, Y.-F. Chang, C.-H. Wu, and M.-C. Wu, "High-speed light-emitting diodes emitting at 500 nm with 463-MHz modulation bandwidth", *IEEE Electron Device Letters*, vol. 35, no. 5, pp. 563–565, May 2014. DOI: 10.1109/LED.2014.2304513.

[22] A. Supriyanto, Maya, E. S. Rosa, Y. Iriani, A. H. Ramelan, and F. Nurosyid, "Influences mass concentration of P3HT and PCBM to application of organic solar cells", *J. Phys.: Conf. Ser.*, vol. 776, art. 012012, 2016. DOI: 10.1088/1742-6596/776/1/012012.

[23] W. Wang, Y.-H. Lin, R.-S. Guan, T.-C. Wen, T.-F. Guo, and G.-B. Lee, "Bulk-heterojunction polymers in optically-induced dielectrophoretic devices for the manipulation of microparticles", *Opt. Express*, vol. 17, no. 20, pp. 17603–17613, 2009. DOI: 10.1364/OE.17.017603.

[24] T. lvaniga and P. lvaniga, "Evaluation of the bit error rate and Q-factor in optical networks", *IOSR J. Electron. Commun. Eng.*, vol. 9, no. 6, pp. 1–3, 2014. DOI: 10.9790/2834-09610103.

[25] W. Freude *et al.*, "Quality metrics for optical signals: Eye diagram, Q-factor, OSNR, EVM and BER", in *Proc. of 14th Int. Conf. Transparent Opt. Networks*, 2012, pp. 1–4. DOI: 10.1109/ICTON.2012.6254380.

[26] M. Galal, W. P. Ng, R. Binns, and A. Abd El Aziz, "Experimental characterization of RGB LED transceiver in low-complexity LED-to-LED link", *Sensors*, vol. 20, no. 20, p. 5754, 2020. DOI: 10.3390/s20205754.

[27] G. Morthier, G. Roelkens, and R. Baets, "Optical versus RF free-space signal transmission: A comparison of optical and RF receivers based on noise equivalent power and signal-to-noise ratio", *IEEE Journal of Selected Topics in Quantum Electronics*, vol. 28, no. 2, pp.

1–8, id. 3129250, Mar. 2022. DOI: 10.1109/JSTQE.2021.3129250.

[28] S. B. S. Lee, H. Liu, K. S. Yeo, J.-M. Chen, and X. Yu, "Design of differential variable-gain transimpedance amplifier in 0.18 µm SiGe BiCMOS", *Electronics*, vol. 9, p. 1058, 2020. DOI: 10.3390/electronics9071058.

[29] P. Corral, F. Rodríguez-Mas, J. L. Alonso, J. C. Ferrer, and S. Fernández de Ávila, "A low-cost visible light communications system based on organic photodetection for transmitting images", *Engineering Proceedings*, vol. 6, no. 1, p. 85, 2021. DOI: 10.3390/I3S2021Dresden-10116.